Journal of Hazardous Materials 223–224 (2012) 53–62

Contents lists available at SciVerse ScienceDirect

Journal of Hazardous Materials

journal homepage: www.elsevier.com/locate/jhazmat

Aminopropyl-modified mesoporous silica SBA-15 as recovery agents of Cu(II)-sulfate solutions: Adsorption efficiency, functional stability and reusability aspects

M.V. Lombardo[a], M. Videla[b], A. Calvo[c], F.G. Requejo[c], G.J.A.A. Soler-Illia[a,d,*]

[a] Gerencia Química, Centro Atómico Constituyentes, CNEA, Av. General Paz 1499 (B1650KNA), San Martín, Buenos Aires, Argentina
[b] Rhein Chemie Argentina, Luis María Drago 1555 - (B1852LGS) Burzaco, Buenos Aires, Argentina
[c] INIFTA-CONICET, Universidad Nacional de La Plata, CC 16 Sucursal 4 (1900), La Plata, Argentina
[d] DQIAyQF, FCEN, Universidad de Buenos Aires, Ciudad Universitaria, Pab. II (C1428EHA), Buenos Aires, Argentina

ARTICLE INFO

Article history:
Received 12 December 2011
Received in revised form 30 March 2012
Accepted 20 April 2012
Available online 27 April 2012

Keywords:
Mesoporous materials
Ion scavenging
Hybrid adsorbents
Aminopropyl function
Sol–gel
Water treatment
Reusable adsorbent

ABSTRACT

Hybrid mesoporous materials are potentially useful for metal ion scavenging and retrieval because of their high surface areas, controlled accessibility and tailored functionalization. Some aspects that are linked to the performance of HMM include pore accessibility, stability of the organic functions and reusability. Knowledge of these aspects is critical in the design of adsorption–desorption protocols. In this work we produce and characterize propylamino-substituted large pore silica (SBA-15-N), which is submitted to Cu(II) adsorption from copper sulfate solutions, followed by desorption in acid media and material regeneration. We find that the hybrid material is an efficient adsorbent (1.15–1.75 mmol Cu(II) g^{-1}), although a fraction of the organic groups is lost during the adsorption process. An X-ray photoelectron spectroscopy (XPS) study demonstrates that the contents of amino groups are higher in the material surface, leading to different behaviors in Cu(II) complexation along the material. These materials can be regenerated by exposure to acidic media. Thermal processing of the hybrid materials leads to better durability in aqueous solutions during reprocessing, due to enhanced polycondensation of the inorganic framework. Thermally treated samples, once regenerated, are efficient adsorbents in a second step of Cu(II) adsorption. We discuss the materials processing factors involved in the improved adsorption of Cu(II), its quantitative release and reusability of the material.

1. Introduction

Metal ion scavenging and retrieval from water is one of the central problems in natural resources management, and has been subject of study in many aspects during the last decade. Heavy metals present in water from industrial applications (including mining, refining and production of textiles, paints and dyes) are pollutants sometimes present in very low concentrations. A wide variety of techniques to remove these chemical species are available, such as ion exchange, reverse osmosis and nanofiltration, precipitation, coagulation/co-precipitation and adsorption [1]. This last technique is one of the most effective and several approaches have been developed for aqueous efficient separation and remediation. Materials tested include natural or synthetic inorganic solids (zeolites, clays, metal oxides), natural organic matter (polysaccharide-based materials), biosorbents [2], as well as advanced materials such as functional polymers, organic-inorganic hybrids, porous carbons, etc. [3]. Nanoparticle-based materials are potentially interesting adsorbents due to their high surface to volume ratios, although they present limitations associated with their size and dispersability:

(a) Nanoparticle packing leads to the loss of the effective exchange area and high pressure drops, limiting their use in compact reactors.
(b) Handling, retrieval or separation of nanoparticles from slurries is difficult.
(c) Nanoparticles are highly reactive, and tend to readily dissolve under real operation conditions.
(d) Potential health hazards due to dealing with reactive dispersed species.

In this context, mesoporous materials present an advantage: their high specific surface area (200–1500 m^2/g) is contained within the material, which is generally in the shape of micronic or submicronic particles, which are easier to process into columns, for

* Corresponding author at: Gerencia Química, Centro Atómico Constituyentes, CNEA, Av. General Paz 1499 (B1650KNA), San Martín, Buenos Aires, Argentina. Tel.: +54 11 6772 7032; fax: +54 11 6772 7886.
E-mail address: gsoler@cnea.gov.ar (G.J.A.A. Soler-Illia).

0304-3894/$ – see front matter © 2012 Elsevier B.V. All rights reserved.
http://dx.doi.org/10.1016/j.jhazmat.2012.04.049

example. Their porosity in the nanometer scale (2–50 nm) should grant accessibility to the surface, while keeping a robust framework. Therefore, silica-based organic–inorganic hybrids and, more recently, ordered mesoporous organosilica materials have been developed for adsorption procedures [4–6].

Silica-based templated materials with organized, large-size monodisperse mesopores [7,8] display high specific surface areas in the order of 600–1000 m^2/g and highly controlled porous structures (up to 1 cm^3/g or even more) [9]. A functionalized hybrid material can be achieved combining sol–gel techniques, self-assembly of appropriate surfactant and selective surface modification with specific organic functions [10–12]. This kind of composites is attractive since they combine in a single solid phase both the properties of a rigid three-dimensional silica network and the particular chemical reactivity of the organic component [13]. A great variety of mesoporous functional adsorbents have thus been described in the literature, either organically modified mesoporous oxides or periodic mesoporous organosilica [14,15]. However, the use of these sophisticated materials in real situations is limited by their cost. Therefore, interest in robust, reusable adsorbents is growing. Functionalized mesoporous adsorbents are interesting phases, because of their inorganic skeleton that can withstand adverse environmental conditions, as well as repeated adsorption–regeneration cycles. Most of the reported work deals with the synthesis and characterization of the adsorbent hybrid material, and the testing of a variety of heavy metals, kinetics of the processes and eventually the selectivity between different metals [16–19]. Fewer efforts are dedicated to explaining the actual mechanism of adsorption/desorption, and, more importantly, the mechanisms of degradation of the material under operation conditions, which is essential to their reusability [10,11,14,15,20,21]. Among the mesoporous silica materials, SBA-15 (Santa Barbara Amorphous), prepared using poly(alkene oxide) triblock-copolymer as structure directing agent, has large pores and robust thick walls that make it an ideal candidate for designing general purpose adsorbents once functionalized with organic groups or even polymers [8,22–24].

In this work, we produce and characterize propylamino-substituted SBA-15 (SBA-15-N). We test the material towards Cu(II) adsorption, followed by desorption in acid media and regeneration. We find that a fraction of the organic groups is lost during the adsorption process, but improved material stability is gained by thermal processing. Chemical analysis of the bulk material and X-ray photoelectron spectroscopy (XPS) characterization of the surface indicate that the surface and interior of the materials present a different behavior towards Cu(II) adsorption. We discuss the factors involved in the adsorption of Cu(II), its quantitative release and the regeneration process in the reusability of the material, focusing on aspects that are relevant in the design of a practical adsorbent.

2. Experimental

2.1. Synthesis of SBA-15, SBA-15-N and SBA-15-N-T

Preparation of the SBA-15 sample was performed following the method reported by Zhao et al. [8] 12.6 g of Pluronic P123 (Aldrich) was dissolved in 89.6 g of water with stirring at 38 °C. The temperature was lowered to 35 °C following the addition of 359.6 g of 2 M HCl solution (prepared from 37% fuming hydrochloric acid, Merck) and 25.6 g of tetraethyl orthosilicate (TEOS, Fluka, 98%). The solution was kept under stirring at 35 °C for 20 h. The mixture was aged at 90 °C for 24 h without stirring. The solid product was recovered by filtration; it was washed with water several times and once with ethanol, then it was dried at 60 °C. Calcination was carried out by increasing temperature from room temperature to 500 °C for 8 h and kept at 500 °C for 6 h (SBA-15).

The amino-containing hybrid material was obtained by post-grafting in dry toluene (Merck). 1.4 g of SBA-15 was dispersed in 150 ml of toluene and refluxed under stirring. Then 1.6 g of 3-aminopropyltriethoxysilane was added (APTES, Fluka 98%), and the mixture was refluxed for 24 h. The solid product was recovered by filtration; and later washed with toluene and ethanol. Finally, the product was dried at 60 °C for 24 h (SBA-15-N). In order to test the effect of mild thermal treatment in the robustness of the adsorbent, samples of SBA-15-N were heated at 130 °C for 48 h, obtaining a temperature-aged sample, which will be referred to as SBA-15-N-T.

2.2. Characterization

SAXS patterns were obtained at the D02A-SAXS 2 beamline of Laboratório Nacional de Luz Síncrotron (LNLS), Campinas, Brazil, using a sample to detector distance of 750 mm and $\lambda = 1.608$ Å, and an area detector (MARCCD). The XRD signal was processed (radial integration and normalization with respect to dark noise and blank samples) using the Fit-2D software (ESRF) [25]. Nitrogen adsorption–desorption isotherms at 77 K were measured by using a Micromeritics ASAP 2020 equipment. Surface area was calculated by using the BET equation. The total pore volume was obtained at $P/P_0 = 0.99$, and the micropore volume was calculated by *t*-plot. As the observed Type IV isotherms presented Type I hysteresis loops, pore size was obtained from the desorption branch by means of the BJH model [26]. Diffuse reflectance infrared Fourier transform spectroscopy (DRIFTS) measurements were performed with a Nicolet Magna 560 instrument, equipped with a liquid nitrogen cooled MCT-A detector. Thermal analysis was performed with a Shimadzu TGA-50 under oxygen atmosphere. Elemental analysis was performed at UMYMFOR, Buenos Aires, with an Exeter Analytical CE440 Elemental Analyzer equipment. XPS measurements were performed at D04A-SXS line at LNLS, using photon incident energy $l = 1840$ eV with a 45° detection angle. Quoted binding energies were referenced to the adventitious C 1s emission at 285 eV. Measurements were conducted on powdered samples using a conducting double stick carbon tape.

2.3. Copper adsorption–desorption experiments

Copper sulfate ($CuSO_4$) was chosen to test adsorption/desorption processes because sulfate is a very common counterion in wastewater. Adsorption experiments were performed as follows: 50 ml of $CuSO_4$ aqueous solution of varying concentrations (7–300 ppm) were stirred in presence of 100 mg of the suspended powders (SBA-15, SBA-15-N and SBA-15-N-T) at room temperature for 24 h. It is well known that adsorption kinetics is very rapid [27,28]; it was thus assumed that equilibrium was achieved after this period.

Initial solution pH was 5.5 due to the copper contents, representing a reasonable value for natural water. Adsorption experiments at constant pH values of 5.0, 6.0 and 6.3 were carried out in aqueous solutions using a Metrohm 655 Dosimat Automatic Burette Titrator Component. The pH was regulated externally by addition of 0.1 M NaOH or 0.1 M H_2SO_4. After preliminary results, it was decided to perform adsorption experiments without pH regulation. The final pH values in the latter case were in the range of 6.5–10.0, depending on the initial copper concentration. Under these non-buffered conditions, it was reported that hybrid mesoporous matrices presented maximum adsorption, and their sorption capacity values were approximately constant in this range [29].

After adsorption, the solids (SBA-15-N A and SBA-15-N-T A) were recovered by centrifugation of the suspensions and the copper content in the supernatant solution was analyzed by atomic

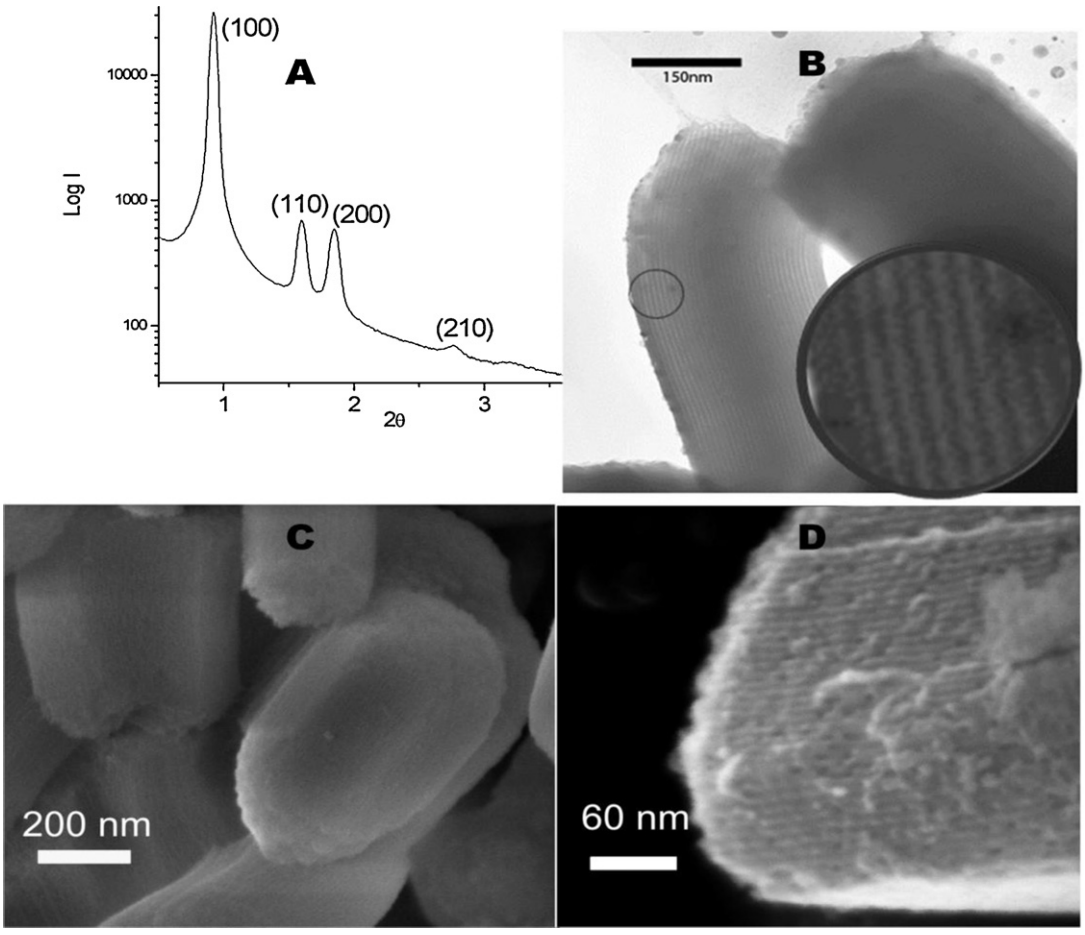

Fig. 1. (A) Integrated SA-XRD pattern obtained for an SBA-15 sample. The inset shows the original SAXS pattern. FE-SEM micrographs of typical SBA-15 particles (B) and zoom of a particle, displaying the channel-like pattern along the longer axis (C) TEM micrograph of typical SBA-15 particles. Inset: 5× magnification of the circular zone depicted in the left particle; channels are clearly observed (D).

absorption spectroscopy (AAS) (Perkin Elmer AAnalyst 100 atomic absorption spectrometer).

Desorption was performed in acidic conditions. The hybrid material with adsorbed copper was immersed into 20 ml of solution of HCl at pH 2.0 under stirring for 2 h. Again, solids (SBA-15-N D and SBA-15-N-T D) were recovered by centrifugation and the copper content in the supernatant solution analyzed by AAS.

The extracted solids were subsequently washed with an alkaline solution in order to regenerate the ion complexing ability of the amino groups. After overnight stirring a suspension of 70 mg hybrid silica in 70 ml of NaOH solution of pH 10.0, the equilibrated solution pH was between 7 and 8. The adsorbent solid was recovered by filtration and was dried prior to use in a second cycle.

In order to test the adsorption capacity after one cycle of adsorption/desorption, 35 ml of 10 ppm $CuSO_4$ aqueous solution were stirred in presence of 70 mg of the suspended regenerated powders (i.e. samples after NaOH treatment) at room temperature for 24 h. The powder was recovered by centrifugation (SBA-15-N A2 and SBA-15-N-T A2) and the copper content in the supernatant solution was analyzed by AAS.

3. Results and discussion

3.1. Synthesis and characterization of the mesoporous hybrid matrices

High quality SBA-15 powder was obtained by precipitation, after controlled hydrolysis-condensation of silica in acidic medium in the presence of P123 template, as described in Section 2.

SAXS patterns of calcined SBA-15 powders show a high degree of ordering, presenting at least six peaks due to the mesostructure (Fig. 1A). Peak distance ratios correspond well with a 2D hexagonal structure (space group *p6m*), details of the indexing are supplied in the ESI.

The cell parameter (a) obtained from Eq. (1) is 10.7 nm for the calcined SBA-15 sample (see ESI). An identical 2D hexagonal ordering with similar mesostructure distance parameters is found for functionalized SBA-15-N and SBA-15-N-T powders (see ESI).

Electronic microscopy micrographs presented in Fig. 1B–D confirm the high mesoscale order of the produced samples. Elongated particles of 700 ± 50 nm length and 400 ± 40 nm width were observed by FE-SEM. Higher magnifications permit to observe channel-like structures running parallel to the longer direction. These channels correspond well to 2D hexagonal structure typical of SBA-15, as confirmed by TEM.

Nitrogen adsorption isotherms obtained at 77 K of pure and organically modified mesoporous samples are presented in Fig. 2. Type IV curves with H1 hysteresis loops are obtained in all the samples, in good agreement with the well-known behavior of SBA-15 [30]. Table 1 presents the BET surface area, the total pore volume calculated by Gurvitch method, the micropore volume calculated by *t*-plot Harkins–Jura–Boer (mesopore volume = total pore volume − micropore volume) and pore diameter calculated by the BJH method, for all three materials studied in this work. The APTES contents measured by elemental analysis and estimated by TGA (15% loss due to organic material, see ESI) is also shown, both techniques giving coincident values of ca. 2 mmol of organic function per gram

Table 1
Pore features of SBA and amino-substituted SBA samples.

	Surface area (m^2/g)	Total volume (cm^3/g)	Micropore volume (cm^3/g)	Mesopore volume (cm^3/g)	Pore diameter (nm)	mmol APTES/g[a]	mmol APTES/g[b]
SBA-15	737	0.85	0.05	0.80	5.8	–	–
SBA-15-N	344	0.52	0.002	0.52	5.0	2.0	1.97
SBA-15-N-T	332	0.49	0.001	0.49	5.1	–	1.92

[a] Results by thermogravimetric analysis.
[b] Results by elemental analysis.

of mesoporous matrix, i.e., a N:Si atomic ratio of 0.13 for hybrid samples with or without thermal treatment.

It can be observed that upon addition of the organic functions, the surface area falls practically to half of the initial value, and pore volume of the modified samples is ca. 60% of the initial pore volume. Pore diameter is in turn diminished from 5.8 to 5.0 nm. The decrease in pore radius cannot fully account for the observed decrease in surface area and pore, suggesting that at least partial pore plugging takes place. Microporosity is also diminished in the hybrid samples, suggesting that in the soft conditions used for functionalization, condensation of APTES takes place preferentially at the pore surface, filling the micropore cavities.

FTIR measurements (Fig. 3) were performed in order to characterize the silica-based matrices, and in particular, the incorporation of organic functions to the pore systems. All spectra present the typical Si–O–Si bands of the inorganic framework Si–O–Si bands: transverse optical Si–O–Si modes (TO) in the 800 cm^{-1} (ν_s, or TO_2 mode) and in the 950–1300 cm^{-1} zone (ν_{as}, or TO3 mode, and a longitudinal optical mode, appearing as a shoulder at 1250 cm^{-1}) for all samples [31]. The absorbance of the Si–O–H bands at 960 cm^{-1} in pristine SBA-15 turns into a shoulder upon functionalization, indicating that the aminosilane groups are substituting surface silanols. The presence of organic groups is confirmed by ν_{C-H} bands in the 2800–3000 cm^{-1} region, broad ν_{N-H} stretching bands superimposed to those of water, in the 3000–3500 cm^{-1} range and bending C–H between 1300 and 1500 cm^{-1} [32]. A detail of the O–H and N–H bending zone in the 1500–1700 cm^{-1} region is presented in Fig. 3B. The observed bands correspond to δ_{O-H} of adsorbed water (1650 cm^{-1}), and δ_{N-H} of free or protonated amino groups (asymmetric $N-H^+$ bending at 1560 cm^{-1} and N–H bending at 1590 cm^{-1}). The presence of large N–H vibrations is typical of N-containing species with a strong H-bonding interaction with the pore surface [33]. Amino groups are equilibrated with ammonium-silanolate pairs, as demonstrated by the presence of the bending bands of the protonated and unprotonated species [34]. Although no quantitative speciation information could be obtained from these bands, these results are consistent with previous data obtained in APTES-post-grafted mesoporous silica by XPS [35] or in hybrid sol–gels by MAS-NMR [36].

In conclusion, the method reported here permitted to produce SBA-15-type mesoporous powders of submicronic size presenting well aligned channels of ca, 5.8 nm diameter, and 2 mmol N g^{-1} amino functions (N:Si ratio of ca. 0.13).

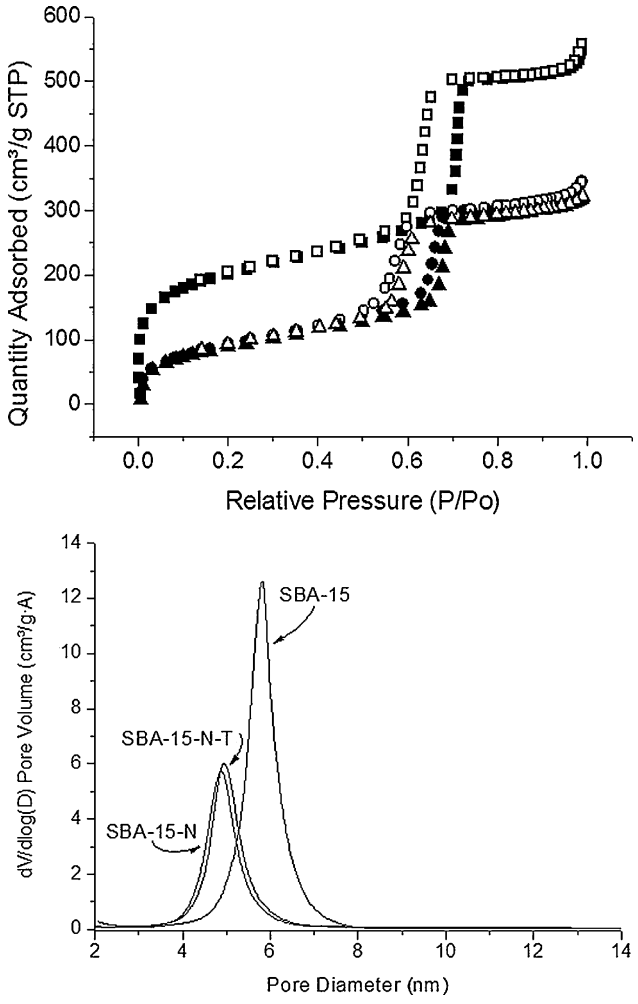

Fig. 2. Upper: nitrogen adsorption (closed)–desorption (open) curves for SBA-15 (■), SBA-15-N (●) and SBA-15-N-T (▲). Lower: pore size distributions obtained from the desorption branch of the nitrogen isotherms, for SBA-15, SBA-15-N and SBA-15-N-T.

3.2. Copper(II) adsorption

Cu(II) adsorption experiments performed under constant pH show an increase in the adsorption capacity when pH increases from 5.0 to 6.3. If the pH is not regulated externally, a pH increase from 5.5 to 6.5 is observed after adsorption, and the Cu^{2+} uptake is slightly higher than the one observed at pH 6.3 (Fig. 4). When pH is increased above 6.5, $Cu(OH)_2$ precipitation takes place for Cu(II) concentrations above 50 ppm. Therefore, detailed experiments were performed in non-regulated conditions in order to maximize adsorption in highly reproducible conditions (i.e., in the absence of copper hydroxide precipitate).

Full adsorption isotherms were obtained from equilibrium experiments performed in the presence of copper concentrations between 7 and 300 ppm. Fig. 5A shows that while no significant adsorption takes place in the pure mesoporous silica matrix in the explored conditions, significant copper quantities are incorporated into the pore systems of the amino-functionalized materials. This highlights the role of the amino function as a copper scavenger, in line with the current literature [1,3,5,10,13]. In addition, the isotherms corresponding to the hybrid adsorbents show a sharp initial slope indicating a high adsorption efficiency of the modified mesoporous silica for low copper concentrations. For example, no signal corresponding to remaining Cu^{2+} is detected after

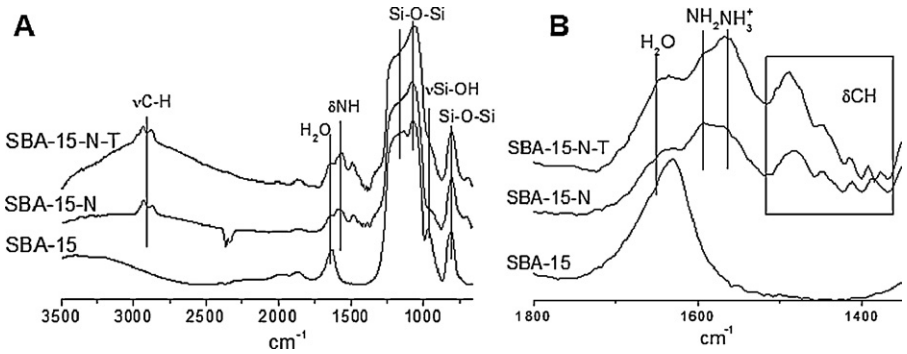

Fig. 3. (A) FT-IR spectra of SBA 15, SBA-15-N and SBA-15-N-T in the 800–3250 cm^{-1} region; (B) detail of the 1350–1800 cm^{-1} region, showing the N–H and O–H bending bands of purely inorganic and hybrid samples.

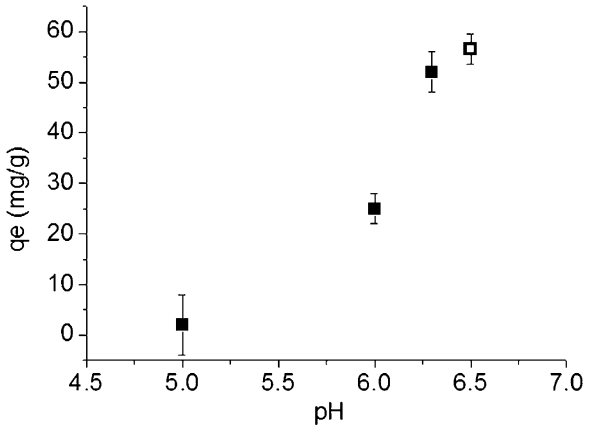

Fig. 4. Adsorption of Cu(II) ions in conditions of regulated pH (closed) and non-regulated pH (open). The Cu^{2+} adsorption capacity improves as the pH increases ($CuSO_4$ solution 100 ppm).

equilibration of the adsorbent with a 7 ppm solution (the detection limit for AAS is 0.2 ppm).

The adsorption data were adjusted according to a Langmuir isotherm, Eq. (2)

$$q_e = \frac{Q_0 b C_e}{1 + bC_e} \quad (2)$$

where q_e is the actual Cu(II) loading in the mesoporous material, C_e is the external equilibrium Cu(II), Q_0 is the maximum adsorption capacity, i.e. the amount of metal to form a monolayer, and b is a constant related to the intensity of adsorption [1]. Correlation factors of $r^2 > 0.997$ were obtained; therefore, this simple model was judged valid enough for comparison with literature values. The Langmuir expression can be linearized in the form $C_e/q_e = (1/Q_0 b) + (C_e/Q_0)$ (Fig. 5B), leading to Q_0 values of 73.5 ± 0.7 and 111 ± 2 mg Cu(II) g^{-1} adsorbent, and b values 0.02 ± 0.01 and 0.03 ± 0.01 L/mg for SBA-15-N and SBA-15-N-T, respectively (i.e., Q_0 values of 1.2 and 1.7 mmol Cu(II) g^{-1} adsorbent, respectively). These maximum loading values are in line with previous findings on post-grafted MCM-41-derived samples [37], and significantly higher than those reported in post-grafted [29] or co-condensed SBA-15 at a comparable temperature [38], all of them in the range 0.35–0.85 mmol Cu(II) g^{-1} [20]. Even if both types of samples present similar N:Si ratios, the higher maximum adsorption capacity of the SBA-15-N-T sample can be attributed to the rearrangement of the inorganic network that takes place upon thermal treatment. Aminosilane surface groups tend to present intense interactions with the silica surface; however, these chains present some mobility, and the surface is quite dynamic [39]. Silane condensation that occurs after submitting the samples to temperatures in the range of 150 °C can lead to disrupt the H-bonding interactions between the amino groups and the surface silanols, improving the amino group exposure on the pore surface [36].

Elemental analysis of the whole samples performed after copper adsorption gave an N:Si ratio of 0.07 for SBA-15-N and 0.08 for SBA-15-N-T, and Cu:N ratios of 1.07 for SBA-15-N and 1.56 for SBA-15-N-T. These data indicate two relevant points: (a) a significant fraction of the amino functions (46.5% and 22%, respectively) is lost in the first adsorption process, and (b) under these conditions, a ratio of more than one copper to nitrogen atom is obtained in saturated samples. The first effect is due to partial dissolution of surface amino groups that takes place above neutral pH values, such

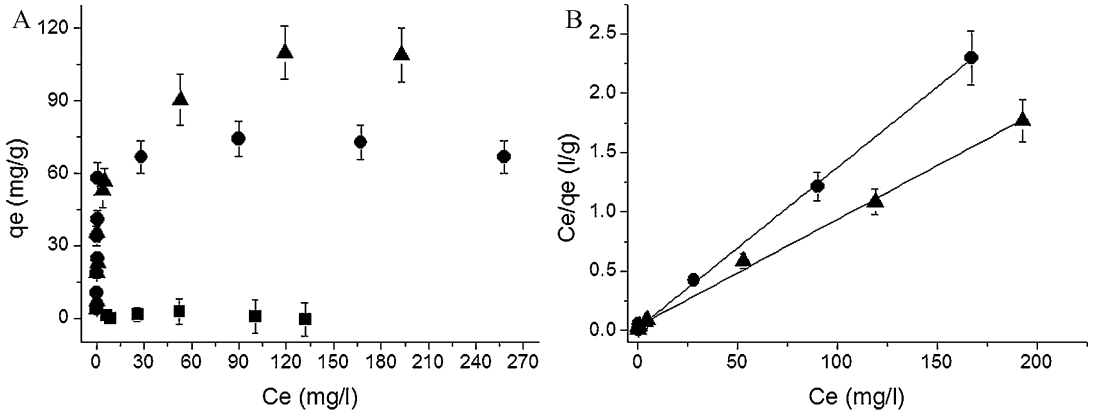

Fig. 5. (A) Adsorption isotherms of Cu(II) sulfate solutions onto mesoporous silica or hybrid matrices: SBA-15 (■), SBA-15-N (●), SBA-15-N-T (▲); (B) linearization of adsorption data according to the Langmuir model for the hybrid matrices.

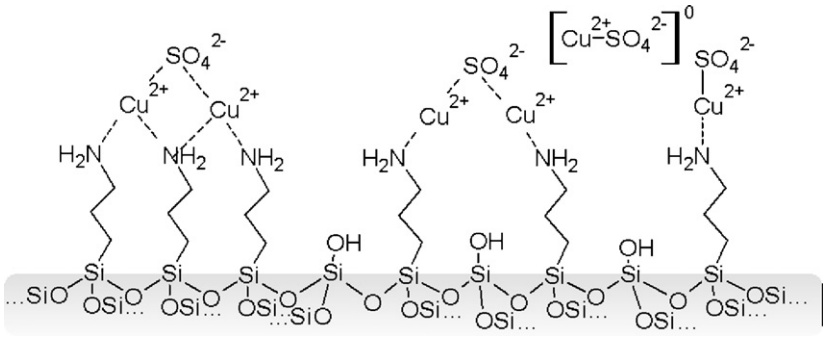

Scheme 1. Possible coordination of copper ions by functionalized matrix, and stabilization by sulfate anions.

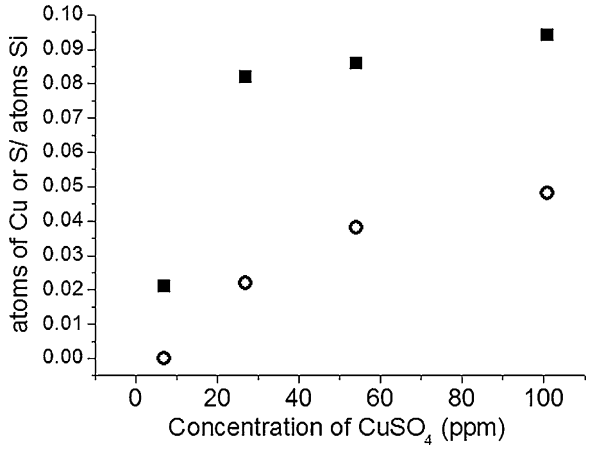

Fig. 6. Cu:Si (■) and S:Si (○) atomic ratios obtained by EDS for SBA-15-N samples exposed to solutions containing variable initial copper concentration.

as those attained in non-buffered experiments as those presented here [20,34]. The second can be explained by the well known fact that ion adsorption in hybrid mesoporous matrices depends on the type of counter anion. Lam et al. demonstrated that the enhanced copper uptake in the pore systems of amino-MCM 41 (up to 30%) was due to stabilization of the Cu(II) charge by SO_4^{2-} that generates neutral species able to interact with amino or silanol surface groups, as depicted in Scheme 1 [37].

Energy dispersive spectroscopy (EDS) measurements on copper-loaded hybrid matrices exposed to solutions with variable Cu(II) concentrations are presented in Fig. 6. A consistent S:Cu relationship of ca. 0.5 is obtained for all analyzed samples, indicating that SO_4^{2-} are co-adsorbed with Cu^{2+} ions.

In addition, adsorption kinetics is very fast; the initially white material turned blue immediately after contact with the copper containing solutions. Preliminary kinetic experiments (see ESI) show that after 3 h contact, it can be safely considered that equilibrium is reached. Recent work performed in a similar hybrid mesoporous material obtained by co-condensation led to conclude that adsorption kinetics follows generally a pseudo-second order law [1,40], as a result of the contribution of different adsorption-migration paths for the ions: i.e., a rapid initial adsorption on external and highly available sites, followed by copper diffusion within the pores (intraparticle diffusion). This results in a relatively complex mechanism that is dependent on variables such as pH or temperature, as demonstrated by Da'na et al. [28], in which typical equilibration times are in the order of 30 min to 1 h, in line with our findings.

In order to shed light into the homogeneity of the distribution of the organic groups and its consequences on the adsorption properties of the hybrid matrices, XPS studies were conducted on hybrid samples, whether in pristine form, exposed to Cu(II) solutions, or to regenerating process (see below). Due to the density of this kind of mesoporous silica and the energy of the incident photons, the analysis depth is estimated in ca. 10 nm [35]. Representative Si, Cu and N XPS spectra for the thermally treated samples (i.e. SBA-N-T) along an adsorption (A1)–desorption (D1)–reloading (A2) cycle are presented in Fig. 7. Full data comparing bulk composition (obtained by AAS and elemental analysis) and surface composition (obtained by XPS) are gathered in Table 2.

XPS Si 2p spectra show a characteristic peak at 104 eV that corresponds to silicon dioxide [41], which remains constant along all adsorption and desorption steps, indicating that no significant changes can be detected at the surface structure. In N 1s spectra, two superimposed peaks at 400 and 402 eV shows the presence of amino (399.5 eV) and ammonium (401.2 eV) groups on silica surface for the initial hybrid samples, in good agreement with the FTIR

Table 2
Comparison of bulk and surface composition by XPS and elemental analysis.

	N:Si		Cu:N	
	Bulk[a]	XPS (±10%)	Bulk[b]	XPS (±10%)
SBA-15-N	0.13 ± 0.02	0.43 ± 0.04	–	–
SBA-15-N A1 (250 ppm)[c]	0.07 ± 0.01	0.20 ± 0.02	1.07 ± 0.12	0.78 ± 0.08
SBA-15-N D1	0.05 ± 0.01	0.24 ± 0.02	0.00 ± 0.01	0.05 ± 0.01
SBA-15-N A2 (10 ppm)	0.02 ± 0.01	0.12 ± 0.01	0.00 ± 0.01	0.00 ± 0.01
SBA-15-N-T	0.13 ± 0.02	0.34 ± 0.03	–	–
SBA-15-N-T A1 (100 ppm)[d]	0.08 ± 0.02	0.23 ± 0.02	0.80 ± 0.08	0.61 ± 0.06
SBA-15-N-T D1	0.07 ± 0.01	0.22 ± 0.02	0.09 ± 0.02	0.05 ± 0.01
SBA-15-N-T A2 (10 ppm)	0.04 ± 0.01	0.18 ± 0.02	0,20 ± 0.02	0.38 ± 0.04

[a] Obtained by elemental analysis.
[b] Obtained comparing adsorbed Cu(II) per gram adsorbent and N from elemental analysis.
[c] Data corresponding to the saturation zone of the isotherm.
[d] Data corresponding to the low concentration zone of the isotherm.

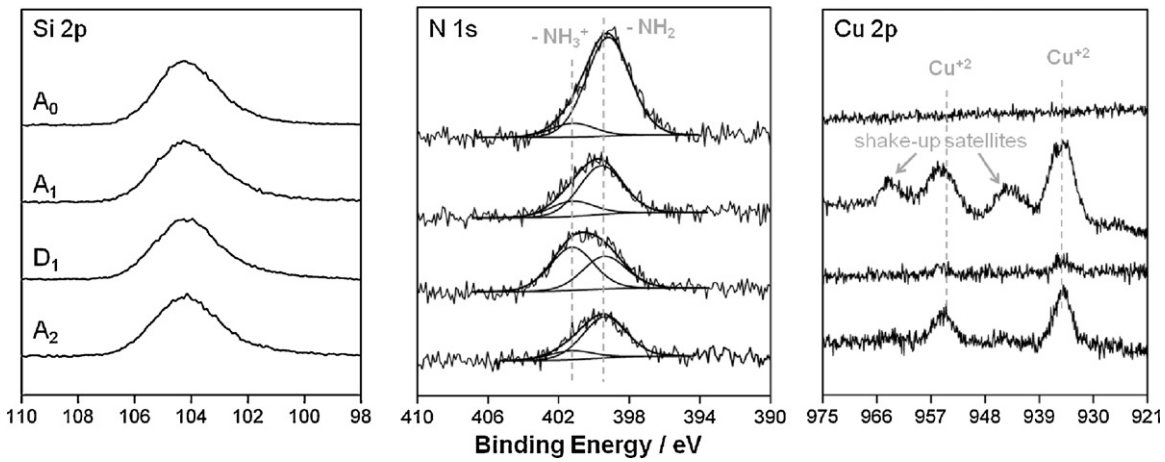

Fig. 7. Representative XPS spectra of hybrid SBA-N-T samples, for Si 2p (left), N 1s (center) and Cu 2p (right). Curves correspond to pristine SBA-15-N-T (A_0), SBA-15-N-T-A1 (A_1), SBA-15-N-T-D1 (D_1) and SBA-15-N-T-A2 (A_2). See Table 2 for more details.

spectra and previous XPS information [42]. It can be qualitatively observed that the ammonium:amino signal ratio increases after desorption (step D1), indicating that copper is substituted by protons. Normalized signals show a decrease in intensity after the first Cu absorption, this fact can be explained by the loss of functional groups upon adsorption (see below). Cu 2p spectra indicate that Cu^{+2} is successfully incorporated to the hybrid material surface in the first absorption (SBA-15-N-T-A1 in Fig. 7), presenting a characteristic 2p doublet ($2p_{1/2}$ and $2p_{3/2}$ peaks) and the two satellites indicated with arrows [43]. The observed peaks at 935 and 955 eV are well in the region of Cu(II) species. The absence of satellites at 946 and 961 eV in the Cu 2p spectrum of SBA-15-N-T-A2 sample could be attributed to Cu(I) species, but no reduction is likely in these conditions. We rather prefer to attribute them to a different coordination (see below); a detailed XAS study is underway to delve with this issue.

From Fig. 7 and Table 2, it can be clearly seen that the amino groups concentration is larger on the particle surface than in the interior of the particles, under all conditions. For example, in the initially produced hybrid materials (SBA-15-N), the surface concentration of amino groups is more than three times the average one. This effect is well known in mesoporous powders or xerogels produced by post-grafting [44], and it can lead to a function gradient or even pore blocking. Noteworthily, when samples are heated, the ratio of surface to bulk N atoms decreases, suggesting that a more even distribution can be attained. It has been proposed that migration of grafted functional groups in mesopores can take place through a desorption–diffusion–adsorption sequence [45]. This has also been observed in the case of organosilanes bound to silica surfaces. In this case, surface migration proceeds through a hydrolyzed intermediate that rebinds to adjacent silanol sites on the silica surface, the barrier to surface diffusion being the hydrolysis of the surface siloxane bond [46]. While reported lateral diffusion coefficients are modest, the activation energy of 16.3 kcal/mol can be overcome by temperature, which seems to be the case here.

After the first copper adsorption step (i.e. samples N-A1 and N-T-A1), incorporation of Cu(II) and loss of amino functions were observed, as discussed above. Roughly half of the amino functions are lost at the particle surface sites during the adsorption process, which is a similar fraction with respect to the total amino loss. Measures of Cu(II):N ratio at the surface (XPS) are slightly lower than those of the overall particle obtained by AAS and elemental analysis, suggesting that the transport of a small size ion such as copper along the pore systems is easier than diffusion of a larger, more reactive molecule such as APTES. The lower Cu:N ratios at the surface also indicate that average coordination of Cu(II) by amino groups is higher than in the particle interior, probably between 1 and 2 amino groups per Cu(II); the satellite peaks might indicate a different environments for the metallic center, probably a site with lower coordination, due to the lack of enough amino groups to achieve a 2:1 N:Cu ratio, a phenomenon that has been already observed in hybrid sol–gel materials [47].

3.3. Copper(II) desorption and reutilization of the mesoporous matrix

To test the desorption properties, the Cu-loaded hybrid materials were suspended in acid solution (HCl, pH 2) and stirred for 2 h. Suspensions were subsequently centrifuged and copper content in the supernatant was analyzed by AAS. Fig. 8 shows the Cu(II) desorption (expressed as Cu(II) moles retrieved in the acid solution with respect to the copper initially adsorbed in the material) for systems with different initial copper concentrations. All values are in the 90–100% range, and no significant differences in copper uptake and release were observed between hybrid samples that have been submitted or not to thermal treatment. An almost complete disappearance of the copper XPS peaks shows a successful desorption of the Cu(II) from the silica matrices, except for a small fraction that still remains bound, probably with a high coordination. However,

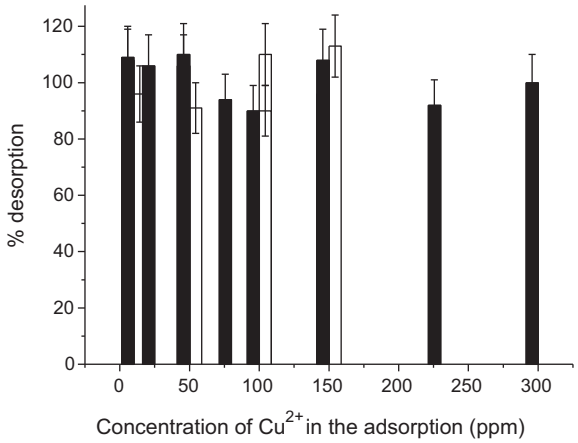

Fig. 8. Fraction of copper ions desorbed from hybrid samples SBA-15-N (black) and SBA-15-N-T (white), after an adsorption step in the presence of variable copper concentrations.

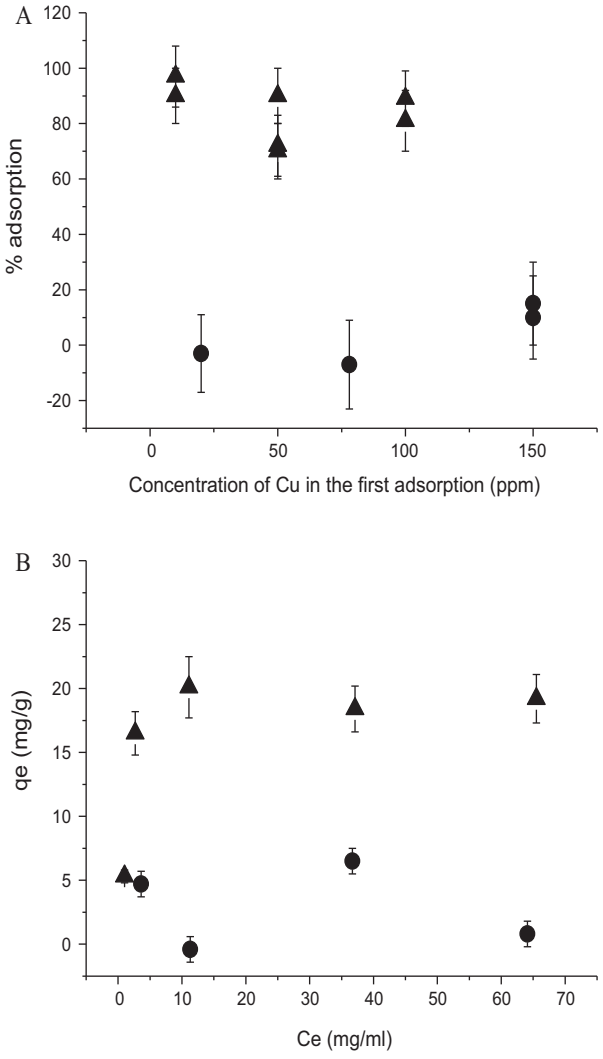

Fig. 9. (A) Fraction of copper ions adsorbed (10 ppm) in hybrid samples SBA-15-N (●) and SBA-15-N-T (▲), after a first adsorption–desorption procedure, for samples that have been exposed to different copper concentrations in the first step. (B) Second adsorption isotherms of Cu(II) sulfate solutions onto hybrid matrices: SBA-15-N (●), SBA-15-N-T (▲). The adsorption data of SBA-15-N-T were adjusted according to a Langmuir isotherm. Correlation factors of $r^2 = 0.997$ and $Q_0 = 20 \pm 1$ mg Cu(II) g^{-1} adsorbent were obtained.

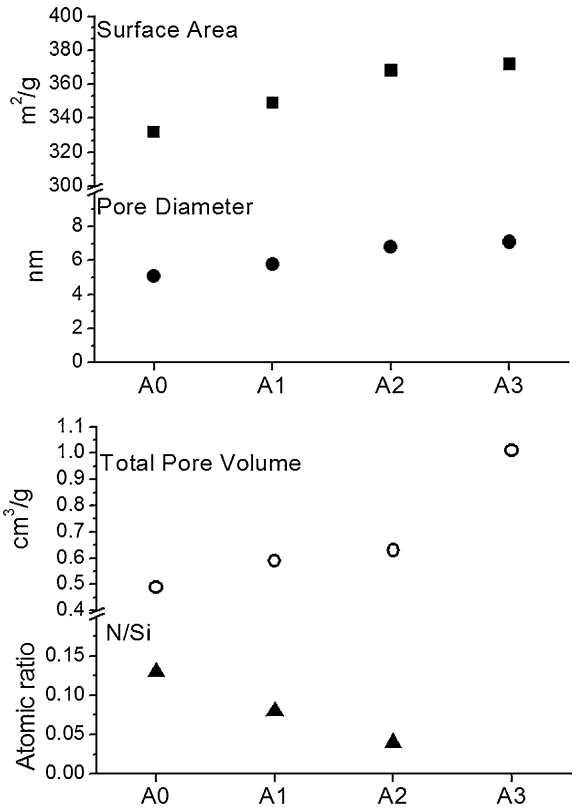

Fig. 10. Surface area, m^2/g (■), total pore volume, cm^3/g (○), pore diameter, nm (●) and atomic ratio N/Si (▲) at different adsorption steps for SBA-15-N-T.

elemental analysis and XPS show marked differences between N-D and N-T-D samples, amino leaching being more important in the case of non-treated hybrids (ca. 29% versus 13%, respectively).

To test the reusability of these matrices, a second adsorption step after copper desorption was tested. In order to maximize the N:Cu ratio, and to test the possibility of totally removing the metal ions, the adsorbents were put in contact with a low Cu(II) concentration. In a first experiment, 70 mg of materials (SBA-N-D and SBA-N-T-D after NaOH treatment) were put in contact with 35 ml of 10 ppm $CuSO_4$ aqueous solution while stirring. Suspensions were subsequently centrifuged, and copper content in the solution was analyzed by AAS. Fig. 9A shows that in this case, amino-containing samples SBA-15-N present a poor performance in the second Cu(II) adsorption process, irrespectively of the Cu(II) concentration of the first adsorption. On the contrary, samples that have been thermally treated (SBA-15-N-T) permit to recover practically 80–95% of the metal ions adsorbed by the hybrid material in the first step. The experiment was systematically repeated for different Cu(II) concentrations in the second step, permitting to obtain a second adsorption isotherm of Cu(II). Results plotted in Fig. 9B confirm that the SBA-15-N-T samples present a clearly better Cu(II) second adsorption in an ample copper concentration range compared to the non-treated sample. The adsorption data of SBA-15-N-T adjusted according to a Langmuir isotherm yield a value of $Q_0 = 20 \pm 1$ mg Cu(II) g^{-1} adsorbent (correlation factor of $r^2 = 0.997$). This can be explained by the increased stability due to an enhanced Si–O–Si condensation after heating. In addition, FTIR spectra of the mesoporous adsorbents performed after repeated copper loading and desorption cycles (see ESI) show unequivocally that the organic function is rapidly lost in the SBA-N samples, the SBA-N-T samples being much more stable. Interestingly, copper XPS spectra obtained from SBA-15-N-T-A2 samples put in contact with dilute Cu(II) solutions present only one set of peaks, suggesting that at low loadings, a major fraction of copper species with higher coordination is attained (Cu:N ratio <0.5, see Fig. 7 and Table 2).

Silica matrices containing amino functions can suffer from dissolution at the pore surface, and subsequent leaching of the organic functions, due to the nucleophilic character of the amino groups that trigger dissolution of surface silanols [36]. However, it has been demonstrated that a mild thermal treatment enhances durability of sol–gel hybrid matrices towards dissolution [20]. The thermally treated samples are thus more suitable to resist repeated metal loading-unloading cycles. Notwithstanding, deleterious effects of repeated exposure to alternating highly acidic and alkaline conditions are observed. Fig. 10 shows the evolution of surface area, total pore volume, mesopore size and N:Si contents on SBA-15-N-T samples submitted to three adsorption–desorption cycles. It can be observed that nitrogen leaching is linked to the particle dissolution that preferentially takes place at the pore surface at elevated pH. Recent work in the literature permits to anticipate that the use of buffered media, and milder adsorption and pore regeneration procedures such as exposure to carbonate solutions or recycling

with EDTA might be beneficial for adsorbent durability and reusability [38,48].

4. Conclusions

This work demonstrates that amino post-grafted mesoporous silica with channel-like structure is a strong, fast, efficient (1.15–1.75 mmol Cu(II) g^{-1}) and potentially reusable adsorbent for Cu(II) ions, even in dilute solutions. The role of the counter ion (in this case, sulfate) is important, for it mediates in the adsorption behavior of the cation of interest. We demonstrated that the post-grafting procedure leads to high N loadings that take place mostly in the micropores; amino groups accumulate preferentially at the particle surface, probably at the pore entrances, leading to obtain different coordination environments for Cu(II) ions, as assessed by XPS. In addition, we could determine that an important fraction of the aminopropylsilane groups is lost upon Cu(II) adsorption. Importantly, aging the functionalized material at low temperature exposes a higher number of amino dangling groups to the pore surface, and improves their attachment. This is due to an improvement on the silica condensation that results in a higher Si–O–Si cross-linking and therefore, expulsion of amino groups from the silica network. This important aspect demonstrates the relevance of the post-treatment after grafting in the performance, particularly aiming at reusability of these hybrid matrices as ion scavengers. In addition, the submicronic particle size permits a good pore accessibility at the same time that grants adequate packing to form inorganic–organic hybrid membranes that can be of use in actual ion scavenging processes [49].

Acknowledgements

Authors thank ABTLUS for funding access to the LNLS synchrotron facility (proposals D11A-SAXS1-11060 and D04A-SXS-10808). Work funded by ANPCyT (grants PICT 1848, PAE 2004 22711, PME 00038, FONARSEC FSNANO 2010/007). VL thanks CONICET and Rhein Chemie Argentina for a graduate student fellowship. GJAASI is a CONICET staff researcher. Authors thank Dr. M.C. Marchi for her assistance in electronic microscopy measurements, and Drs. H. Westfahl and M. Cardoso for their assistance in SAXS.

Appendix A. Supplementary data

Supplementary data associated with this article can be found, in the online version, at http://dx.doi.org/10.1016/j.jhazmat.2012.04.049.

References

[1] J. Aguado, J.M. Arsuaga, A. Arencibia, M. Lindo, V. Gascón, Aqueous heavy metals removal by adsorption on amine-functionalized mesoporous silica, J. Hazard. Mater. 163 (2009) 213–221.
[2] S. Babel, T.A. Kurniawan, Low-cost adsorbents for heavy metals uptake from contaminated water: a review, J. Hazard. Mater. 97 (2003) 219–243.
[3] See e.g. the themed issue on "Advanced Materials in Water Treatments" D.Y. Zhao, M. Jaroniec, B.H. Hsiao (Eds.), J. Mater. Chem. 20 (2010) 4476ss.
[4] A. Sayari, S. Hamoudi, Periodic mesoporous silica-based organic–inorganic nanocomposite materials, Chem. Mater. 13 (2001) 3151–3168.
[5] F. Hoffmann, M. Cornelius, J. Morell, M. Fröba, Silica-based mesoporous organic–inorganic hybrid materials, Angew. Chem. Int. Ed 45 (2006) 3216–3251.
[6] A. Walcarius, L. Mercier, Mesoporous organosilica adsorbents: nanoengineered materials for removal of organic and inorganic pollutants, J. Mater. Chem. 20 (2010) 4478–4511.
[7] D. Zhao, J. Feng, Q. Huo, N. Melosh, G.H. Fredrickson, B.F. Chmelka, G.D. Stucky, Triblock copolymer syntheses of mesoporous silica with periodic 50 to 300 Angstrom pores, Science 279 (1998) 548–552.
[8] D. Zhao, Q. Huo, J. Feng, B.F. Chmelka, G.D. Stucky, Nonionic triblock and star diblock copolymer and oligomeric surfactant syntheses of highly ordered, hydrothermally stable, mesoporous silica structures, J. Am. Chem. Soc. 120 (1998) 6024–6036.
[9] G.J.A.A. Soler-Illia, C. Sanchez, B. Lebeau, J. Patarin, Chemical strategies to design textured materials: from microporous and mesoporous oxides to nanonetworks and hierarchical structures, Chem. Rev. 102 (2002) 4093–4138.
[10] H. Yoshitake, Design of functionalization and structural analysis of organically-modified siliceous oxides with periodic structures for the development of sorbents for hazardous substances, J. Mater. Chem. 20 (2010) 4537–4550.
[11] J. Liu, X. Feng, G.E. Fryxell, L.-Q. Wang, A.Y. Kim, M. Gong, Hybrid mesoporous materials with functionalized monolayers, Adv. Mater. 10 (1998) 161–165.
[12] G.J.A.A. Soler-Illia, P. Innocenzi, Mesoporous hybrid thin films: the physics and chemistry beneath, Chem. Eur. J. 12 (2006) 4478–4494.
[13] Z. Wu, D.Y. Zhao, Ordered mesoporous materials as adsorbents, Chem. Commun. 47 (2011) 3332–3338.
[14] O. Olkhovyk, M. Jaroniec, Chemically-modified mesoporous silicas and organosilicas for adsorption and detection of heavy metal ions, in: G.E. Fryxell, G. Cao (Eds.), Environmental Applications of Nanomaterials: Synthesis, Sorbents and Sensors, Imperial College Press, London, 2007, pp. 179–212 (Chapter 8).
[15] D. Brühwiler, Postsynthetic functionalization of mesoporous silica, Nanoscale 2 (2010) 887–892.
[16] X. Chen, K.F. Lam, Q. Zhang, B. Pan, M. Arruebo, K.L. Yeung, Synthesis of highly selective magnetic mesoporous adsorbent, J. Phys. Chem. C 113 (2009) 9804–9813.
[17] M. Lui, K. Hidajat, S. Kawi, D.Y. Zhao, A new class of hybrid mesoporous materials with functionalized organic monolayers for selective adsorption of heavy metal ions, Chem. Commun. (2000) 1145–1146.
[18] K.F. Lam, K.L. Yeung, G. McKay, A rational approach in the design of selective mesoporous adsorbents, Langmuir 22 (2006) 9632–9641.
[19] M. Ghoul, M. Bacquet, M. Morcellet, Uptake of heavy metals from synthetic aqueous solution using modified PEI-silica gels, Water Res. 37 (2003) 729–734.
[20] M. Etienne, A. Walcarius, Analytical investigation of the chemical reactivity and stability of aminopropyl-grafted silica in aqueous medium, Talanta 59 (2003) 1173–1188.
[21] E. Da'na, A. Sayari, Adsorption of heavy metals on amine-functionalized SBA-15 prepared by co-condensation: applications to real water samples, Desalination 285 (2012) 62–67.
[22] G.E. Fryxell, The synthesis of functional mesoporous materials, Inorg. Chem. Commun. 9 (2006) 1141–1150.
[23] J.L. Shi, Z.L. Hua, L.X. Zhang, Nanocomposites from ordered mesoporous materials, J. Mater. Chem. 14 (2004) 795–806.
[24] G.J.A.A. Soler-Illia, O. Azzaroni, Multifunctional hybrids by combining ordered mesoporous materials and macromolecular building blocks, Chem. Soc. Rev. 40 (2011) 1107–1150.
[25] Software obtained from the following link: http://www.esrf.eu/computing/scientific/FIT2D/aftp_fit2d.html.
[26] M. Thommes, R. Köhn, M. Fröba, Sorption and pore condensation behavior of pure fluids in mesoporous MCM-48 silica, MCM-41 silica, SBA-15 silica and controlled-pore glass at temperatures above and below the bulk triple point, Appl. Surf. Sci. 196 (2002) 239–249.
[27] A. Benhamou, M. Baudu, Z. Derriche, J.P. Basly, Aqueous heavy metals removal on amine-functionalized Si-MCM-41 and Si-MCM-48, J. Hazard. Mater. 171 (2009) 1001–1008.
[28] E. Da'na, N. De Silva, A. Sayari, Adsorption of copper on amine-functionalized SBA-15 prepared by co-condensation: kinetics properties, Chem. Eng. J. 166 (2011) 454–459.
[29] A.M. Burke, J.P. Hanrahan, D.A. Healy, J.R. Sodeau, J.D. Holmes, M.A. Morris, Large pore bi-functionalised mesoporous silica for metal ion pollution treatment, J. Hazard. Mater. 164 (2009) 229–234.
[30] S. Lowell, Characterization of Porous Solids and Powders: Surface Area, Pore Size, and Density, Springer, 2004, p. 120.
[31] P. Innocenzi, Infrared spectroscopy of sol–gel derived silica-based films: a spectra-microstructure overview, J. Non-Cryst. Solids 316 (2003) 309–319.
[32] G. Socrates, Infrared Characteristic Group Frequencies, 3rd edition, John Wiley and Sons, Chichester, 2001.
[33] D. Brunel, A.C. Blanc, E. Garrone, B. Onida, M. Rocchia, J.B. Nagy, D.J. Macquarrie, Spectroscopic studies on aminopropyl-containing micelle templated silicas. Comparison of grafted and co-condensation routes, Stud. Surf. Sci. Catal. 142 (2002) 1395–1402.
[34] B.V. Zhmud, J. Sonnefeld, Aminopolysiloxane gels: production and properties, J. Non-Cryst. Solids 195 (1996) 16–27.
[35] A. Calvo, M. Joselevich, G.J.A.A. Soler-Illia, F.J. Williams, Chemical reactivity of amino-functionalized mesoporous silica thin films obtained by co-condensation and post-grafting routes, Microporous Mesoporous Mater. 121 (2009) 67.
[36] G.S. Caravajal, D.E. Leyden, G.R. Quinting, G.E. Maciel, Structural characterization of (3-aminopropyl)triethoxysilane-modified silicas by silicon-29 and carbon-13 nuclear magnetic resonance, Anal. Chem. 60 (1988) 1776–1786.
[37] K.F. Lam, X. Chen, G. McKay, K.L. Yeung, Anion effect on Cu^{2+} adsorption on NH2-MCM-41, Ind. Eng. Chem. Res. 47 (2008) 9376–9383.
[38] E. Da'na, A. Sayari, Adsorption of copper on amine-functionalized SBA-15 prepared by co-condensation: equilibrium properties, Chem. Eng. J. 166 (2011) 445–453.
[39] G.E. Fryxell, in: G.E. Fryxell, G. Cao (Eds.), Environmental Applications of Nanomaterials. Synthesis, Sorbents and Sensors, Imperial College Press, London, 2007, p. 167.

[40] Y.-S. Ho, Review of second-order models for adsorption systems, J. Hazard. Mater. B136 (2006) 681–689.
[41] M.J. Edgell, D.R. Baer, J.E. Castle, Biased referencing experiments for the XPS analysis of non-conducting materials, Appl. Surf. Sci. 26 (1986) 129–149.
[42] A. Calvo, P.C. Angelomé, V.M. Sanchez, D. Scherlis, F.J. Williams, G.J.A.A. Soler-Illia, Mesoporous aminopropyl-functionalized hybrid thin films with modulable surface and environment-responsive behavior, Chem. Mater. 20 (2008) 4661–4668.
[43] C.C. Chusuei, M.A. Brookshier, D.W. Goodman, Correlation of relative XPS shakeup intensity with CuO particle size, Langmuir 15 (1999) 2806–2808.
[44] M.H. Lim, A. Stein, Comparative studies of grafting and direct syntheses of inorganic–organic hybrid mesoporous materials, Chem. Mater. 11 (1999) 3285–3295.
[45] P.C. Angelomé, G.J.A.A. Soler-Illia, Organically modified transition-metal oxide mesoporous thin films and xerogels, Chem. Mater. 17 (2005) 322–331.
[46] H. Wang, J.M. Harris, Surface diffusion of organosiloxane ligands covalently bound to silica, J. Am. Chem. Soc. 116 (1994) 5754–5761.
[47] G.V. Kudryavtsev, D.V. Miltchenko, V.V. Yagov, A.A. Lopatkin, Ion sorption on modified silica surface, J. Colloid Interface Sci. 140 (1990) 114–122.
[48] E. Da'na, A. Sayari, Effect of regeneration conditions on the cyclic performance of amine-modified SBA-15 for removal of copper from aqueous solutions: composite surface design methodology, Desalination 277 (2011) 54–60.
[49] (a) C. Boissière, M.U. Martines, E. Prouzet, A. Larbot, On the specific filtration mechanism of a mesoporous silica membrane, prepared with non-connecting parallel pores, J. Membr. Sci. 251 (2005) 17–28;
(b) C. Boissière, M.A.U. Martines, P.J. Kooyman, T.R. de Kruijff, A. Larbot, E. Prouzet, Ultrafiltration membrane made with mesoporous MSU-X silica, Chem. Mater. 15 (2003) 460–463.